Applied Scientific Research **56:** 221–242, 1996.
© 1996 *Kluwer Academic Publishers. Printed in the Netherlands.*

PTV and POD Analysis of the Instabilities in a Quasi Two-Dimensional Convective Flow

MASSIMO MIOZZI and GIORGIO QUERZOLI
Laboratory of Mechanics of Fluids, University of Rome "La Sapienza", V. Eudossiana 18, 00184 Rome, Italy

Received 19 February 1996; accepted in revised form 19 June 1996

Abstract. An investigation is made of the motion of fluid in a transparent rectangular vessel, heated beneath by a line source, using Particle-Tracking Velocimetry. The control parameters are the Rayleigh number (computed by the power supplied to the system), the Prandtl number and the aspect ratio (height to width ratio) of the vessel. When convection starts, two counter rotating rolls occur. For certain values of the control parameters, the flow becomes unstable and the rolls start to oscillate on a plane orthogonal to the line source (natural swaying motion). The Lagrangian description of the velocity fields (i.e. particle trajectories), is extracted. Data are converted from Lagrangian to Eulerian framework and the time evolution is analysed. Perturbations and instabilities of the velocity field (due to thermal anomalies), are observed. They are related to the natural swaying motion of the rolls. The Fourier decomposition is applied in several points of the grid to obtain a spatial portrait of the energy distribution in frequency domain. By means of Proper Orthogonal Decomposition a complete set of orthonormal functions (modes) is evaluated and the flow field is reconstructed using a small number of modes: POD theory states that these modes retain a greater amount of energy than that of any other possible decomposition. Reconstructed velocity fields and the original ones are compared. In this experiment the first eight modes are found to retain more than 80% of the flow kinetic energy.

Key words: Particle-Tracking Velocimetry, Proper Orthogonal Decomposition, convection

1. Introduction

The convection in prismatic vessels has been investigated for many different configurations of the heat source and of the boundary conditions [1]. Let us consider the case where horizontal surfaces are isothermal, side-walls are adiabatic and the heat source is located at the lower part of the vessel. The convective system is then controlled by three fundamental parameters:

- Rayleigh number [2]

$$\mathrm{Ra} = \frac{g\alpha H^3 Q}{\nu\kappa\lambda}\,, \tag{1}$$

- Prandtl number:

$$\mathrm{Pr} = \frac{\nu}{\kappa}\,, \tag{2}$$

- Aspect ratio:

$$\Gamma = \frac{H}{L}, \tag{3}$$

where g is the gravity acceleration, α is the thermal expansion coefficient, Q is the heat generated per unit length of the line source, H and L are respectively the vessel height and width, κ is the thermal diffusivity of the fluid, λ is the thermal conductivity and ν its kinematic viscosity. If the lower surface is uniformly heated, no preferential direction is assigned to the flow, except for the presence of side-walls. In this situation, both two- and three-dimensional flow patterns occur, depending on the control parameters [3, 4]. In the present experiment, upper and lower surfaces are kept at the same, constant temperature and a line source, orthogonal to the front wall of the vessel, is placed just above the lower surface of the vessel. The use of such a source breaks the three-dimensional character of the convective flow: the fluid is forced to rise at the centre of the vessel and to travel along two counter-rotating rolls, filling the whole vessel. When the Rayleigh number is increased, for $\Gamma > 0.2$ and especially for small Prandtl numbers, the two rolls exhibit periodic oscillations in a vertical plane orthogonal to the line source, as numerical [2] and experimental [5] study have confirmed.

Characteristic time scales are introduced:

$$\tau_t = \frac{H^2}{k} \qquad \text{(thermal diffusion time scale)}, \tag{4}$$

$$\tau_\nu = \frac{H^2}{\nu} \qquad \text{(viscous diffusion time scale)}, \tag{5}$$

$$\tau_g = \left(\frac{H}{g\alpha\Delta T}\right)^{1/2} = \frac{1}{N_{\text{bv}}} \qquad \text{(buoyancy effects time scale)}, \tag{6}$$

where N_{bv} is the Brunt–Vaisala frequency and ΔT is the temperature difference between the heat source and the surfaces, Rayleigh and Prandtl numbers can be rewritten in terms of characteristic scales [6]:

$$\text{Ra} = \frac{\tau_t \cdot \tau_\nu}{\tau_g^2}, \tag{7}$$

$$\text{Pr} = \frac{\tau_t}{\tau_\nu}, \tag{8}$$

Several kinds of motion can be defined varying the values of control parameters:

- for $\text{Ra} < \text{Ra}_c$ (where Ra_c is some critical Rayleigh number), at whatever Prandtl number, the flow field is at rest: τ_t is too small, in comparison with τ_g, to determine a global motion; the heat flux is related only to conduction phenomena;
- for larger Rayleigh numbers, at Prandtl numbers greater than unity, temperature gradients are still smoothed very rapidly and buoyancy effects are meaningful only on long time intervals: the flow is steady;

- for much higher Rayleigh numbers, hot and cold regions are definitely separated: their location in respect to external heating and cooling elements have to be considered to show their influence on global motion inside the vessel; the flow field is time dependent and usually oscillatory;
- a further increase in Rayleigh number leads to the turbulent regime.

For a given Rayleigh number, instabilities appear only at low Prandtl numbers: as a matter of fact for low Prandtl numbers, instabilities are basically driven by viscous diffusion when the ratio $(\tau_\nu/\tau_g) = (\mathrm{Ra}/\mathrm{Pr})^{1/2}$ is large [7] and increases as the Prandtl number decreases. The opposite occurs for high Prandtl numbers instabilities are driven by thermal diffusion and by the ratio $(\tau_t/\tau_g) = (\mathrm{Ra} \cdot \mathrm{Pr})^{1/2}$ which increases with Prandtl number [3, 4].

In the present paper, a non-invasive optical method, Particle-Tracking Velocimetry (PTV), is used to define the velocity field of the system at $\mathrm{Ra} = 1.6 * 10^9$ and to clarify the relative physical mechanisms. Proper Orthogonal Decomposition (POD) and Fourier analysis are performed on PTV data to investigate the hidden dynamics of the system. POD is applied to the time series of Eulerian velocity fields: it gives "the best correlated structures" describing the flow. A particular feature of this approach is that no hypothesis have been made about the nature of turbulence and no closure schemes have been adopted: time history of two components of the velocity are given by the Eulerian fields and evolution in time of POD modes is obtained. There are no other examples in literature of such an application on experimental data without frozen turbulence hypothesis.

In this configuration, quasi-bidimensional hypothesis has been made about velocity field in the measurement plane, and observed results confirmed it. Further experiments have been planned to clarify the behaviour of the swaying motion near the end walls, where the velocity approaches zero and three-dimensional motion occur.

In Section 2 the experimental set-up for bidimensional convection and for PTV measurements is described. A review on data processing and on analysis methods is presented in Section 3. Results are given in Section 4. Conclusions and further developments are presented in Section 5.

2. Experimental Set-Up and Velocity Measurements

The convection is generated in a transparent rectangular vessel, by a line heat source, orthogonal to the measurement plane (Figure 1). The vessel is 12.0 cm in width, 6.0 cm in height and 10.4 cm in depth, so that the horizontal aspect-ratio is $\Gamma = 2$. Side-walls are made up of 1.0 cm thick perspex to have an optical access. The heating source is an electrically insulated resistance (0.8 cm in diameter) connected to a stabilized power supply. It is placed 1 cm above the centre line of the lower surface. The upper and lower surfaces are 1.0 cm thick aluminium plates. The temperature of the plates is controlled by two heat-exchangers consisting in a series of counter-flow channels in which constant temperature water flows.

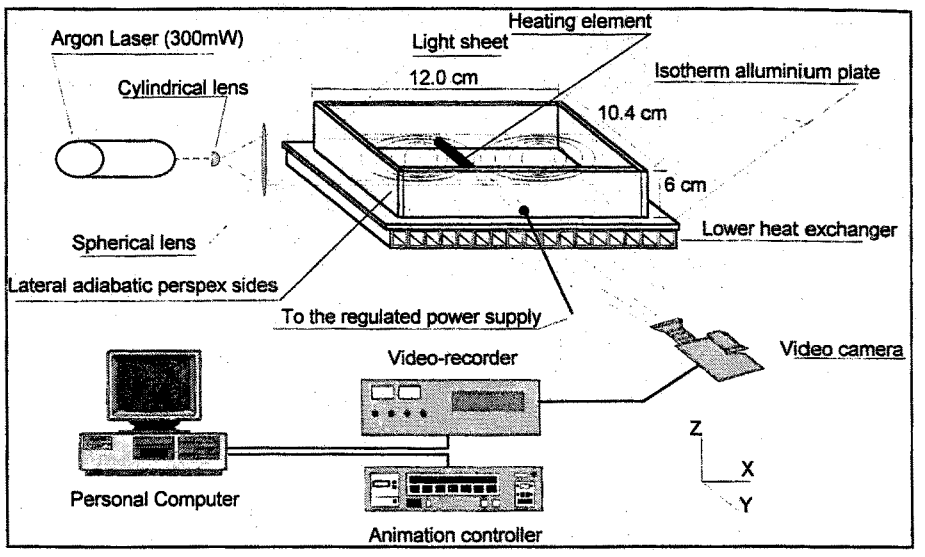

Figure 1. The experimental set-up.

Heat losses are vanishingly small compared to the heat input because temperature differences between working fluid and surrounding ambient are much smaller than those between working fluid and both heat source and isothermal plates.

The velocity measurement is based on tracking of non-buoyant seeding particles uniformly dispersed in the field (Particle-Tracking Velocimetry). The measurement plane, placed at middle depth of the vessel, is illuminated by a light sheet (0.3 cm depth), obtained through a cylindrical lens, from a 300 mW Argon Laser beam. Seeding particles are conifer pollen, $80 \div 120$ μm in diameter. In the PTV the following steps can be observed:

- a series of images is acquired by a CCD video-camera, and recorded on a S-VHS tape at a 25.00 Hz rate; during the recording, an animation controller inserts a frame code on the tape, so that each frame can be individually reached during the off-line analysis;
- one out of every three frames is automatically retrieved using an animation-controller, and digitised by a frame grabber with 512 pixels $\times$ 512 pixels $\times$ 8 bits resolution; the resulting sampling rate is lowered to 8.33 Hz;
- images of seeding particles are recognised on each digitised frame and centroid locations are computed and stored together with the number of the frame where they have been found;
- trajectories of seeding particles are obtained; a temporal series of particle locations is accepted as a trajectory provided that the selected maximum distance between two successive locations and maximum difference between two successive displacements are not exceeded; these criteria are equivalent

to the assumption of a maximum velocity and acceleration in the investigated field;

- the Lagrangian velocity field is evaluated: displacements along trajectories are divided by the time interval between two successive frames and velocity samples are stored together with the location and time at which they are evaluated;
- velocity samples are re-arranged in order to obtain an Eulerian description of the field: velocity samples are reduced to a 10×21 regular grid obtained from 7 successive instantaneous fields.

As a result, the velocity is given on 210 points of the field at a rate of 1.19 Hz. This frequency is much greater than those involved in the convection phenomena under investigation (from previous LDA measurements the integral time scale is about 30 seconds). The acquisition starts after a time lag sufficient for a fully developed regime to be reached and is stopped after 1255 seconds.

3. Data Processing

3.1. From Lagrangian to Eulerian frameworks

The Eulerian velocity field $\mathbf{u}(\mathbf{P}, t)$ is obtained by splitting the measurement area (on which Lagrangian description is given) in 210 (Δx by Δy)-sized, rectangular regions $S(i,j) = \{(x(i) - \Delta x/2 < x(i) < x(i) + \Delta x/2) \cap (y(j) - \Delta y/2 < y(j) < y(j) + \Delta y/2)\}$. The centres $\mathbf{P}(i,j)$ of these areas are used as nodes of the Eulerian representation, giving at $\mathbf{P}(i,j)$, at time t, the mean value of the velocity of all particles that during the time lag $t - \Delta t/2 < t < t + \Delta t/2$ belong to the region $S(i,j)$. In the present experiment, the described parameters are set to be $\Delta x = L/21$, $\Delta y = H/10$ and $\Delta t = 21/25$ s. The number of velocity samples is a function of the position of the node $\mathbf{P}(i,j)$ and of the time t, because particle trajectories are not uniformly described in space and time. Two different explanations can be given: the particles scatter better near the lateral wall through which the light passes first; the particles that seed high velocity regions (i.e. above the heat source) are more than those observed in low velocity regions (i.e. near the corners of the vessel and beside the heat element). In Figure 2 the mean number of samples used at each time to evaluate the velocity in the nodes $\mathbf{P}(i,j)$ is given for the whole grid.

The aim is to extract representative fields that at each instant contain as much data as possible. Two factors play an essential role: the resolution Δx, Δy of the grid and the averaging time Δt. Inverse distance interpolation algorithm is applied to obtain velocity samples on areas where no particles are found: it affects less than 5% of the nodes of the grid at each time.

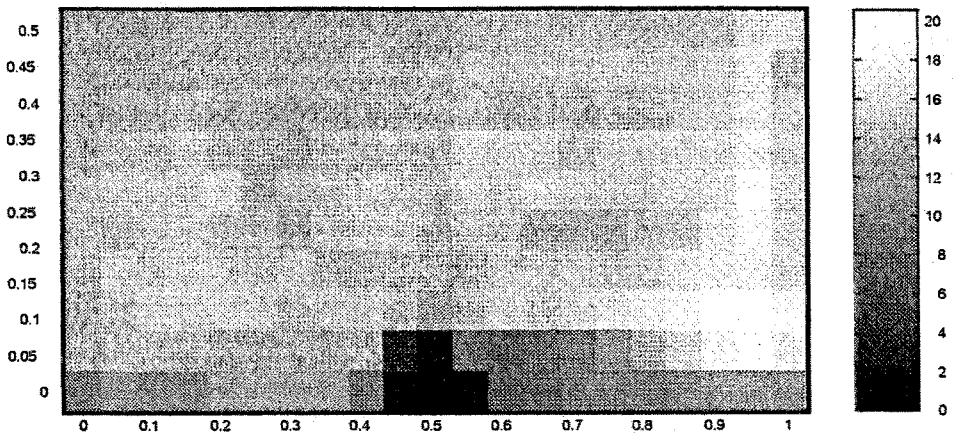

Figure 2. Mean number of samples used to obtain the velocity in the nodes of the grid (21 × 10) each 0.833 seconds.

3.2. Proper Orthogonal Decomposition

The Proper Orthogonal Decomposition is a mathematical tool which permits the extraction of spatial and temporal flow structures from a turbulent field. It provides a rigorous mathematical framework for their description [8]. This tool is in a practical sense without approximations and can be applied to a wide variety of turbulent flows of current interest [9]. This means that the measured velocity fields can be reconstructed completely after decomposition.

Recent developments in turbulence studies point two separate ways: experiments and simulations. There is a lot of information implying the existence of coherent structures and revealing something about their spatial and temporal characters. Recent applications of dynamical system theory to turbulence suggest that such flows reside on relatively low dimensional manifolds or attractors [9–12]. The basic concept is that dissipative systems have relatively low dimensional attractors. Thus, although the phase space for turbulent thermal convection is infinite-dimensional, the trajectory of the system is drawn into a finite dimensional attracting set, as a result of dissipation [13]. The flow may be described with reasonable completeness by the interaction of a relatively few spatial structures [12]. POD is a statistical technique that contributes to deterministic dynamical analysis [8]. The POD decomposition was introduced in the context of turbulence by Lumley [14, 15] and applied to various kinds of fluid-dynamic fields [16–18]. The same tool was applied in other fields with the name of Karhunen–Loève decomposition or principal component analysis and it seems to have been rediscovered several times [9].

Let us consider turbulent, time stationary, convective flows. They are represented by a state vector **v**:

$$\mathbf{v} = (\mathbf{u}, \theta, \rho), \tag{9}$$

where $\mathbf{u}$, ρ and θ are fluctuations of velocity, density and temperature field respectively [9]. For incompressible flows, neglecting the influence of temperature, (9) becomes:

$$\mathbf{v} = \mathbf{u}. \tag{10}$$

Although the physical characters of the problem suggest to many authors the use of $\mathbf{v} = (\mathbf{u}, \theta)$ as state variable for convective problems [9, 10, 13, 22], we will focus the attention only on the fluid motion and on the flow configurations. For our purposes only velocity fields in POD are utilised. The result of decomposition consists of a set of orthonormal functions representing the flow. The state variable $\mathbf{v}$ can be expanded in a set of admissible vector functions $\{\Psi^{(n)}\}$ such as

$$\mathbf{v}_i(\mathbf{x}, t) = \sum_n A^{(n)}(t)\, \Psi_i^{(n)}(\mathbf{x}) \tag{11}$$

and the modal coefficients are uncorrelated:

$$\langle A^k \bar{A}^l \rangle = \lambda_k \delta_{kl}, \tag{12}$$

where angle brackets represent time averaging and the overbar indicates the complex conjugation. The two point spatial correlation tensor can be written as:

$$\mathbf{K}_{ij}(\mathbf{x}, \mathbf{x}') = \langle \mathbf{x}_i(\mathbf{x}, t) \mathbf{v}_j(\mathbf{x}', t) \rangle = \sum_k \lambda_k \Psi_i^{(k)}(\mathbf{x}) \bar{\Psi}_j^{(k)}(\mathbf{x}'). \tag{13}$$

The set $\{\Psi^{(n)}\}$ is usually referred to as "coherent structures" or "modes".

It can be shown that $\mathbf{K}$ is hermitian, non-negative and square integrable (in a physical ground). These properties assure the existence of a unique convergent spectral representation for $\mathbf{K}$ [9]. It means that the $\{\Psi^{(n)}\}$ exist and are unique, forming a complete set of orthonormal functions. Eigenvalues λ_n can be seen as the mean square of the projection of each mode on the velocity field. They have the interpretation of giving the mean energy of the system projected on the Ψ_n-axis in function space. λ_n measures also the average relative time spent by the system along the Ψ_n-axis [9]. The mean energy of the system is given by the sum of the eigenvalues:

$$E = \int \mathbf{K}_{ij}(\mathbf{x}, \mathbf{x}')\, \mathrm{d}\mathbf{x} = \sum_k \lambda_k. \tag{14}$$

POD is optimal in an energetic sense because, among all decompositions, it is the most efficient. The projection on the subspace used for modelling will contain the most kinetic energy possible in an average sense [8]. It means that the amount of energy retained in the subspace (for a given number of modes) is larger than that obtained from any other decomposition.

Three computational steps are used:

- evaluation of the two point correlation matrix:

$$\mathbf{K}_{ij}(\mathbf{x}, \mathbf{x}') = \langle \mathbf{v}_i(\mathbf{x}, t)\mathbf{v}_j(\mathbf{x}', t)\rangle \tag{15}$$

performed on time of all PTV images;

- resolution of the integral equation:

$$\int \mathbf{K}_{ij}(\mathbf{x}, \mathbf{x}')\Psi_i^{(k)}(\mathbf{x}')\, d\mathbf{x}' = \lambda_n \Psi_j^{(k)}(\mathbf{x}) \tag{16}$$

to extract eigenvalues λ_n and eigenvectors $\{\Psi^{(n)}(\mathbf{x})\}$;

- determination of the instantaneous coefficients for the decomposition, $A^{(n)}(t)$:

$$A^{(n)}(t) = \Psi^{(n)}(\mathbf{x}) \bullet \mathbf{v}(\mathbf{x}, t). \tag{17}$$

4. Results and Discussion

4.1. VELOCITY FIELDS

4.1.1. *Mean velocity fields*

The Eulerian field plotted in Figure 3 shows the mean velocity field, averaged over the whole acquisition (1255 seconds), for Ra $= 1.6 * 10^9$. The plume rises in the centre of the tank, above the heating element, and follows the tank travelling along two counter-rotating vortices. Isovalues of horizontal and vertical components of the mean field are also plotted in Figure 3. In the horizontal one, continuous lines are for right-to-left velocities, dotted lines for left-to-right. In the vertical component plot, continuous lines represent downward velocities, dotted lines upward velocities. It can be noted that, with respect to the vertical centre line, the horizontal component is anti-symmetric whereas the vertical one is symmetric.

4.1.2. *Instabilities of the flow and velocity perturbations*

When the Rayleigh number is increased over the threshold, instabilities start and the plume oscillates on a vertical plane (natural swaying motion). This behaviour is shown in Figure 4. The Eulerian fields are taking at $t = 5$ s and $t = 15$ s. At $t = 5$ s the plume is turning on the left, at $t = 15$ s the plume is turning on the right. From 5 to 15 seconds, the plume returns back to the right side.

To clarify the physical reasons for this behaviour, let us briefly refer to the monodimensional convection model [20], in which a loop shaped pipe is heated from below and cooled from above. When the control parameter is small (i.e. for low values of the temperature difference between hot and cold points), the flow is steady and the temperature distribution, after regime conditions have been reached, has uniform values in each arm of the pipe. For higher values of control parameter, hot and cold regions (if compared with the surrounding fluid) are formed near the hot and cold points: they maintain their identity during their revolution along

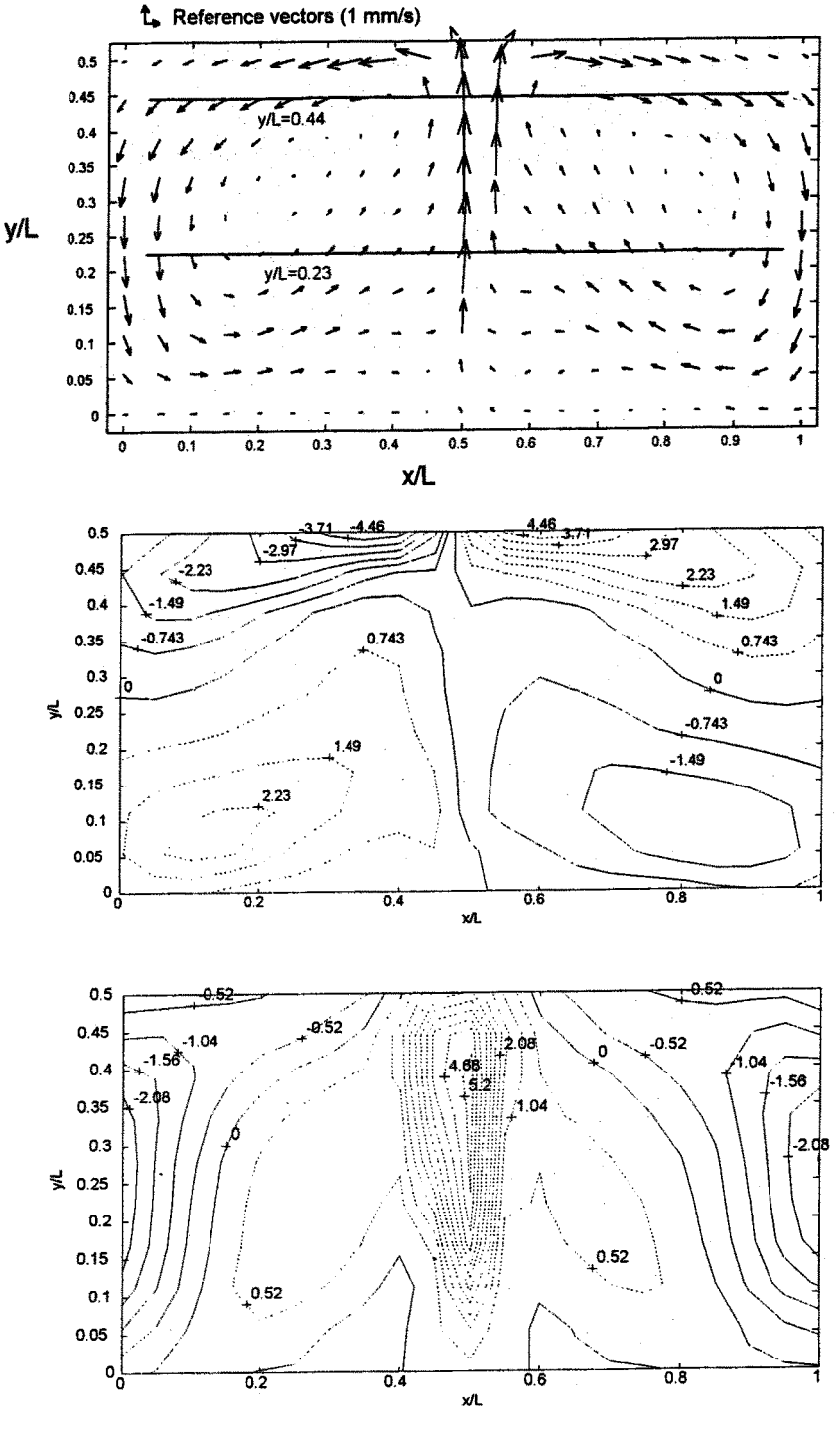

Figure 3. Mean velocity fields. (A) Mean field, (B) mean horizontal field, and (C) mean vertical field.

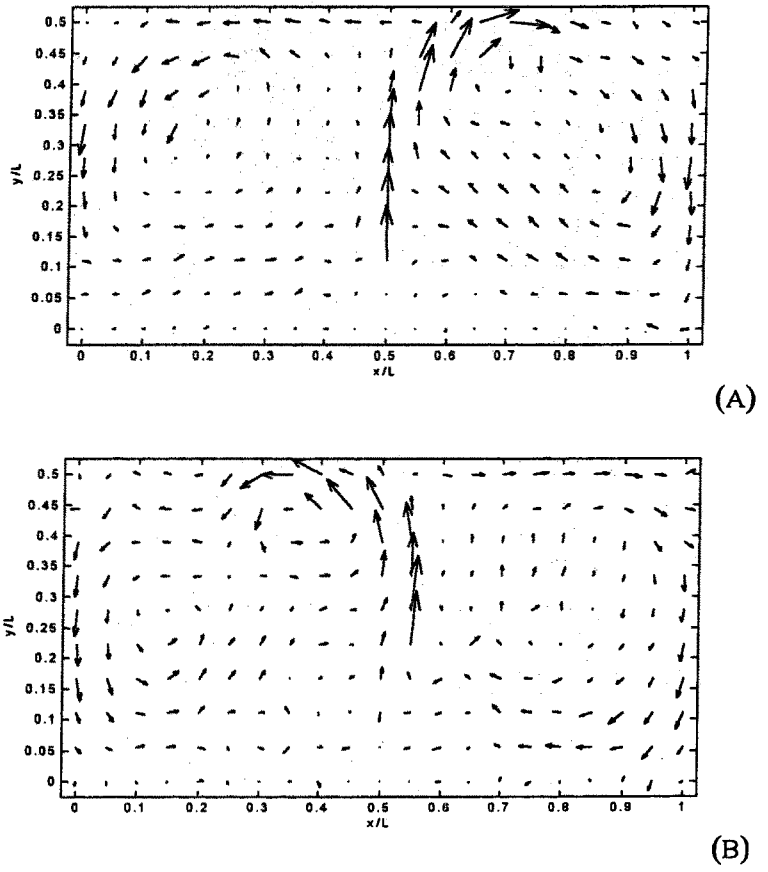

Figure 4. Instantaneous velocity fields. (A) Plume on the right and (B) plume on the left.

the pipe: those regions will be called "blobs". Suppose that a hot blob is formed near the hot point: due to its lower density, it accelerates towards the upper cool region, where its velocity takes the maximum value. At this point it decelerates towards the lower hot region where the velocity is minimum: it generates velocity anomalies. Therefore, the time for the action of heating effects is much longer than that for cooling: the hot blob transfers momentum at each revolution producing oscillations. As a consequence, a feed-back process takes place: the presence of a hot blob enhances oscillation and oscillations increase the hot blob intensity. Similar effects are present for cold blobs.

In Figure 5 the vertical component of the velocity is plotted: isovalues of velocities that in modulus are higher than a fixed threshold are reported. Velocity anomalies are clearly observed rising over the heating element and travelling alternatively on the right side and on the left side of the vessel. These regions of the flow maintain their identity (perturbation of velocity and thermal fields) when

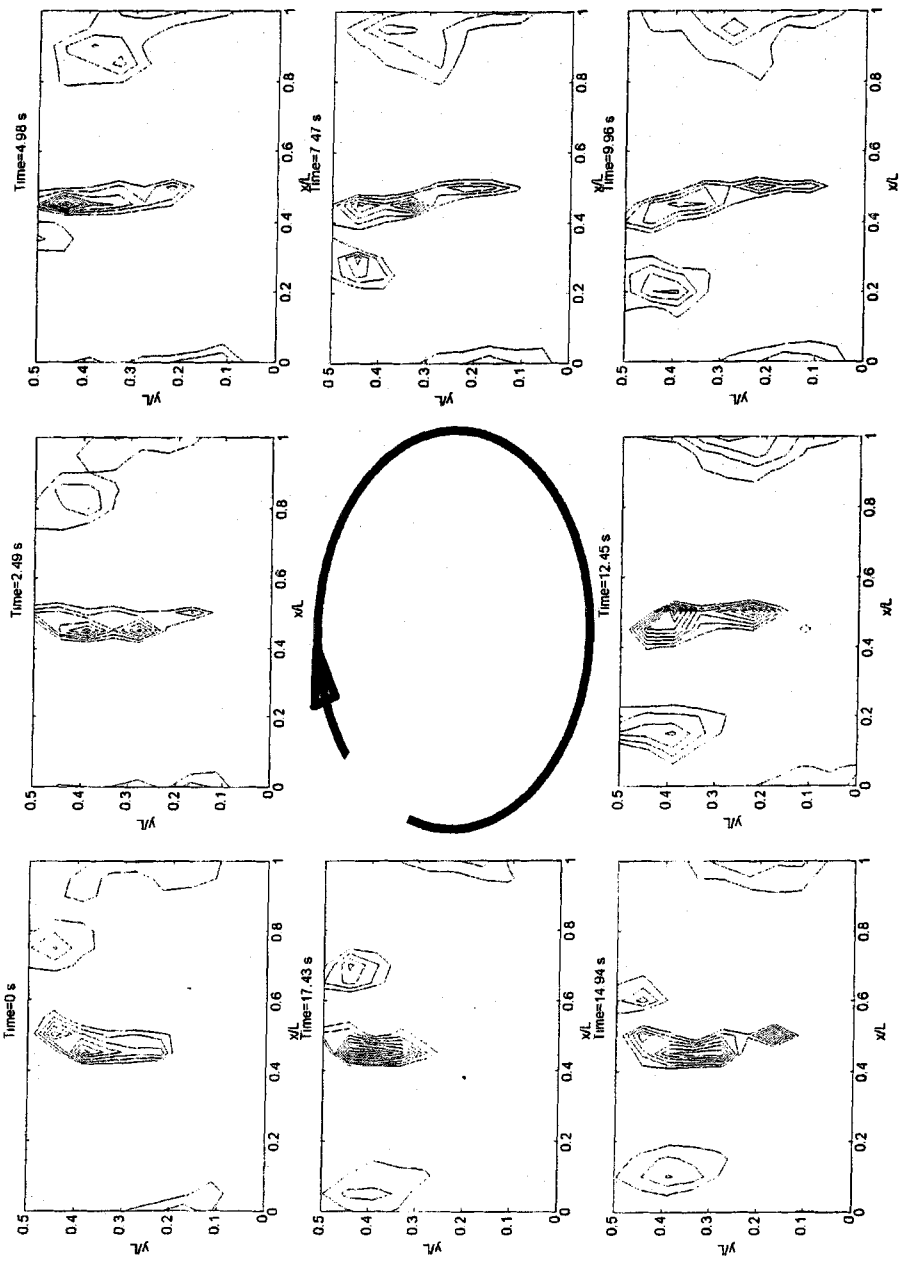

Figure 5. Isovalues of modulus of the vertical component of the velocity higher than a thresold are plotted: Velocity anomalies are travelling alternatively on the right and on the left side of the vessel. Plots are placed clockwise; first one at the top left.

travelling along the rolls, so they transfer momentum to vortices. Instabilities of the rolls are driven by velocity anomalies, related to thermal blobs. They are the assignable cause of the swaying motion of the plume. Successive fields are plotted in clockwise sense to provide a readable representation.

4.1.3. *Fourier analysis, a spatial portrait*

Eulerian velocity fields are obtained at a frequency of 1.19 Hz, much higher than of investigated phenomena. This means that a spectral analysis of velocity time series can be successfully performed at each point of the grid. The power spectra exhibit different characteristics depending on their location. Power spectra of horizontal and vertical velocity components have been evaluated along two horizontal lines, at two different heights: $y/L = 0.42$ and $y/L = 0.23$ and a qualitative description is obtained looking at their contour plots, given in Figure 6. The abscissa represents the horizontal position along the lines at the given level. Frequency is reported on the vertical axis.

The horizontal velocity at $y/L = 0.42$ shows different behaviour between the side and the centre of the vessel. At the side, energy is distributed over a wide range of frequencies, whereas above the heat source, only one peak at 0.0577 Hz is observed. This frequency matches the frequency of oscillation of the plume and corresponds to the life time of the velocity anomalies shown in Figure 5. Vertical velocity spectrum is characterised by two main frequencies along the whole line. The higher corresponds to the inverse of the oscillatory period of the plume (0.0577 Hz) whereas the lower one (0.0172 Hz) is in good agreement with the inverse of the period of fluid particle revolution along a vortex.

At the lower level ($y/L = 0.23$), both plume oscillation and particle revolution frequencies are present in horizontal and vertical velocity spectra. Maxima are located near the centre of the line, above the heat source.

4.2. Proper Orthogonal Decomposition

After Eulerian velocity fields are obtained, POD is performed on the set of data. In Figure 7 the modes from two to four are shown. The first mode is close to the mean field, all the others show different spatial patterns with characteristic structures located at different spatial positions and with different symmetries. POD theory states that using a given number of modes, reconstructed fields retain an amount of energy larger than that of any other decomposition [8]. In other words, a low number of POD modes is sufficient for a good description of instantaneous fields. In Figures 8b and 8c an example of reconstructed fields is plotted. It is to be noted that five modes are sufficient to obtain an overall agreement. Increasing the number of modes up to 25, only a few differences between the original and reconstructed field can be recognised. A quantitative evaluation of the differences

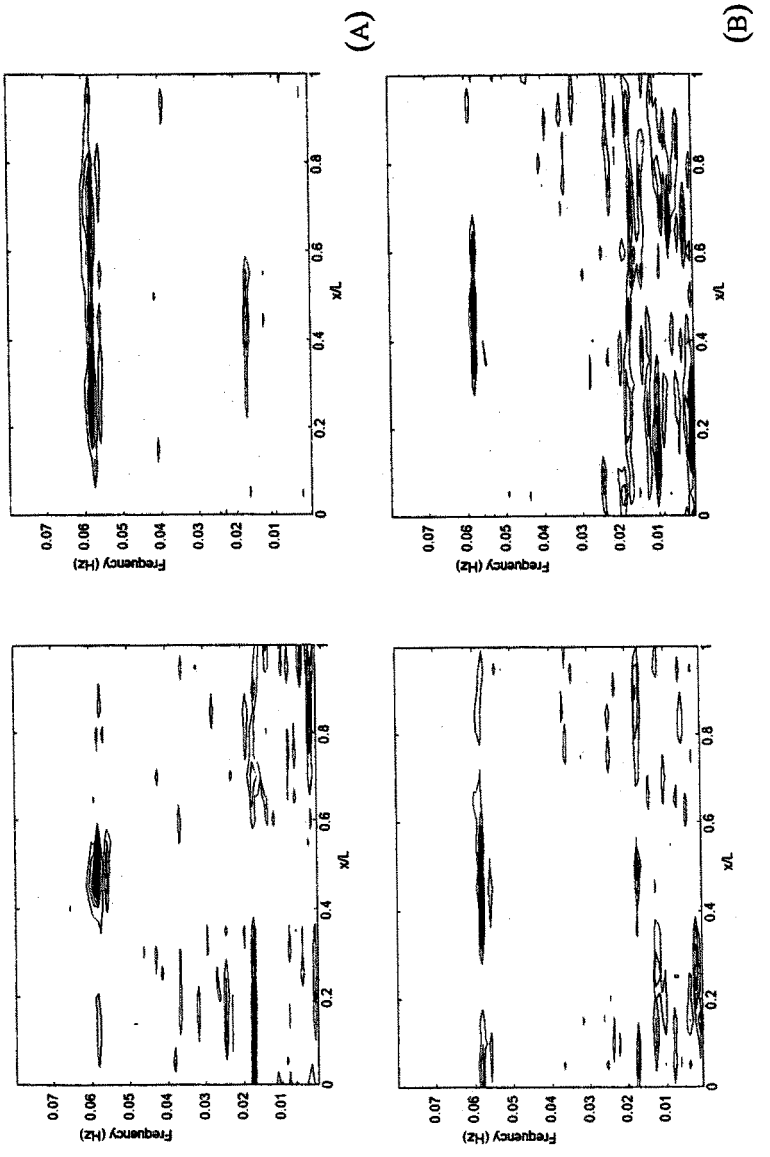

Figure 6. Qualitative spatial portrait of power spectra for horizontal (left) and vertical (right) velocity. (A) Line $y/L = 0.44$ and (B) line $y/L = 0.2$.

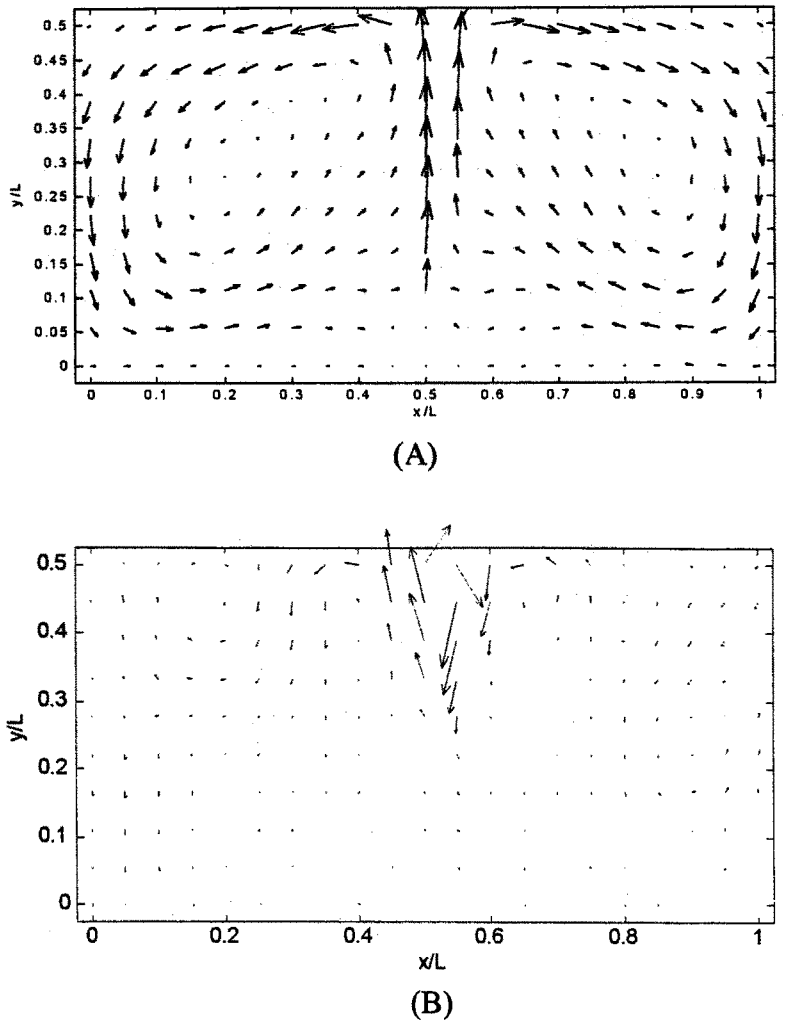

Figure 7. POD first four modes. (A) First mode and (B) second mode.

between the original and the reconstructed fields can be given using the percentage, non-dimensional, mean square error $\varepsilon_{\%}$ defined as:

$$\varepsilon_{\%}(t,n) = 100 \cdot \frac{\left\langle \left[\left(\sum_{i=1}^{n} a^{(i)}(t) \cdot \Psi^{(i)}(\mathbf{x}) \right) - \mathbf{v}(\mathbf{x},t) \right]^2 \right\rangle}{\langle \mathbf{v}(\mathbf{x},t)^2 \rangle},$$

where angle-brackets indicate instantaneous spatial average. In Figure 9a the time averaged behaviour of $\varepsilon_{\%}$ is plotted *versus* the number of modes used to rebuilt the velocity field. Using 200 modes, the averaged value of the percentage error is about 1%. The contour lines corresponding to $\varepsilon_{\%} = 5\%$ and $\varepsilon_{\%} = 15\%$ are plotted

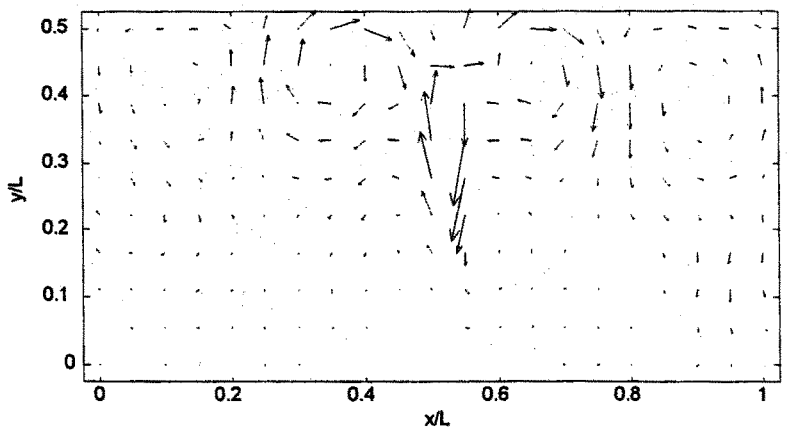

(C)

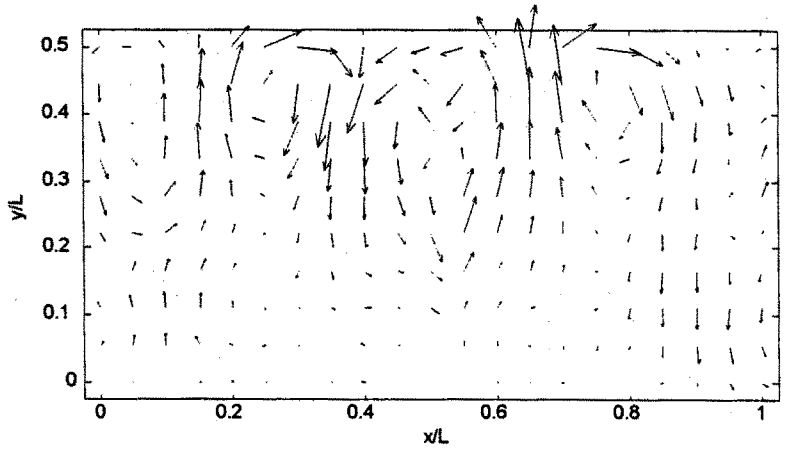

(D)

Figure 7. (C) Third mode and (D) fourth mode.

in Figure 9b. Those contour lines show that the error in the reconstruction of the original instantaneous field is a function both of the number of modes and of the time at which the reconstruction is performed. This is because the eigenfunctions of the correlation matrix are the "most correlated" structures in an average sense, but not at the generic time t. For example, at $t = 310$ s, 50 modes are requested to obtain an error of 5% and at $t = 315$ s, about 150 modes are requested to give the same approximation. It is to be noticed that using the total number of modes, the error disappears.

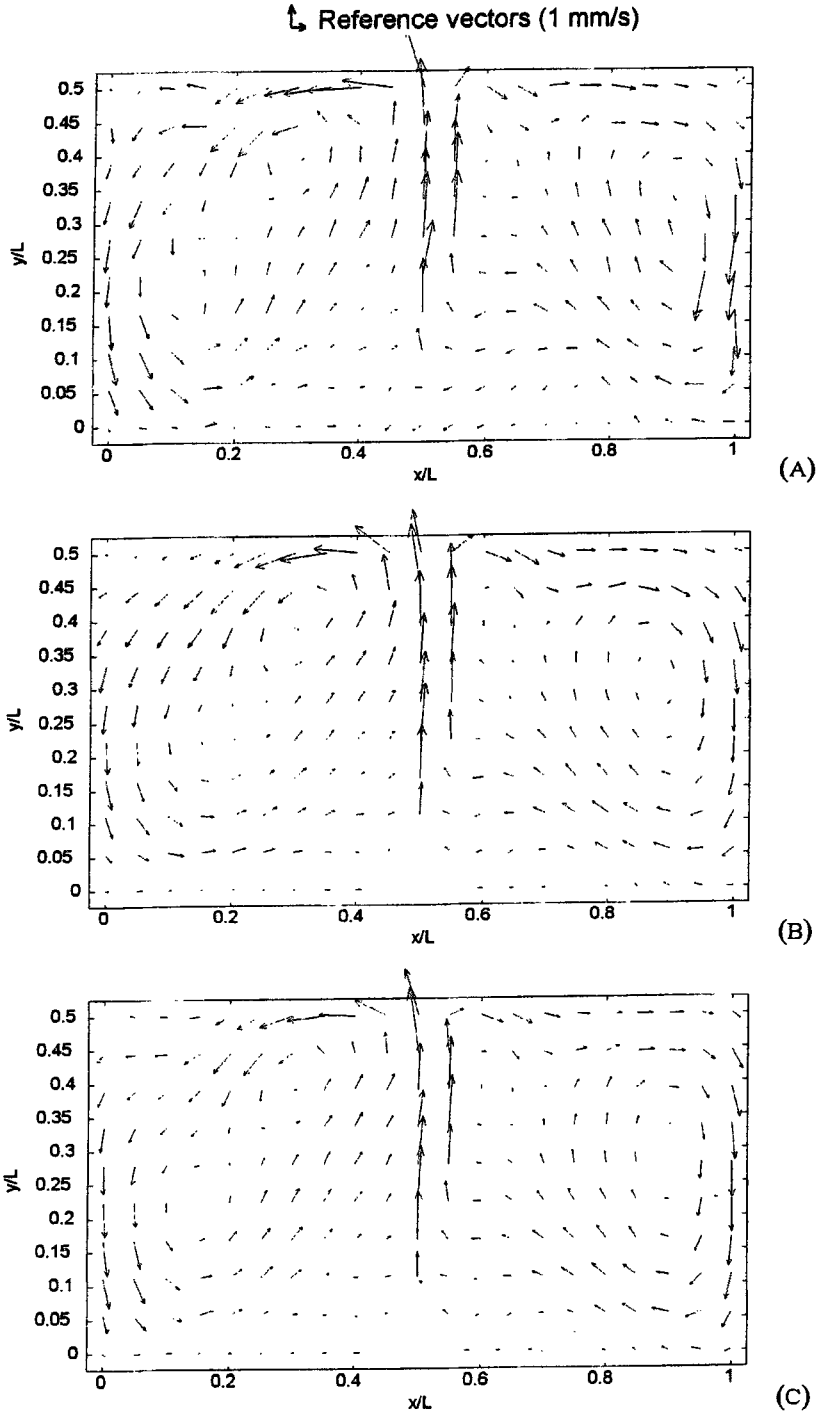

Figure 8. Reconstructed velocity fields. (A) Original velocity field at $T = 126$ s, (B) reconstructed field using 5 modes, and (C) reconstructed field using 25 modes.

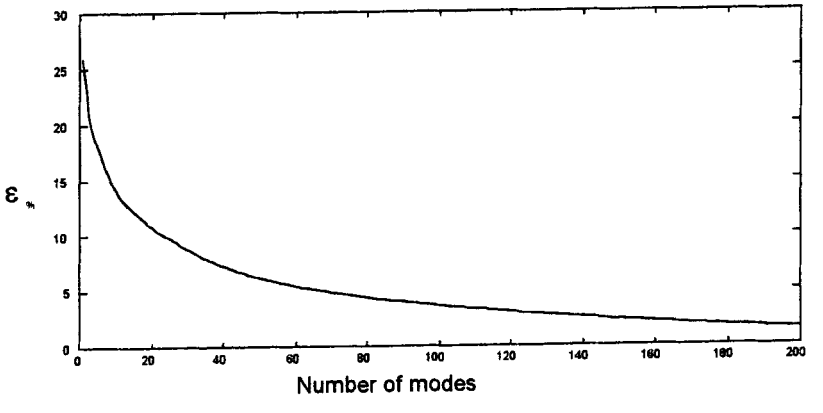

(A)

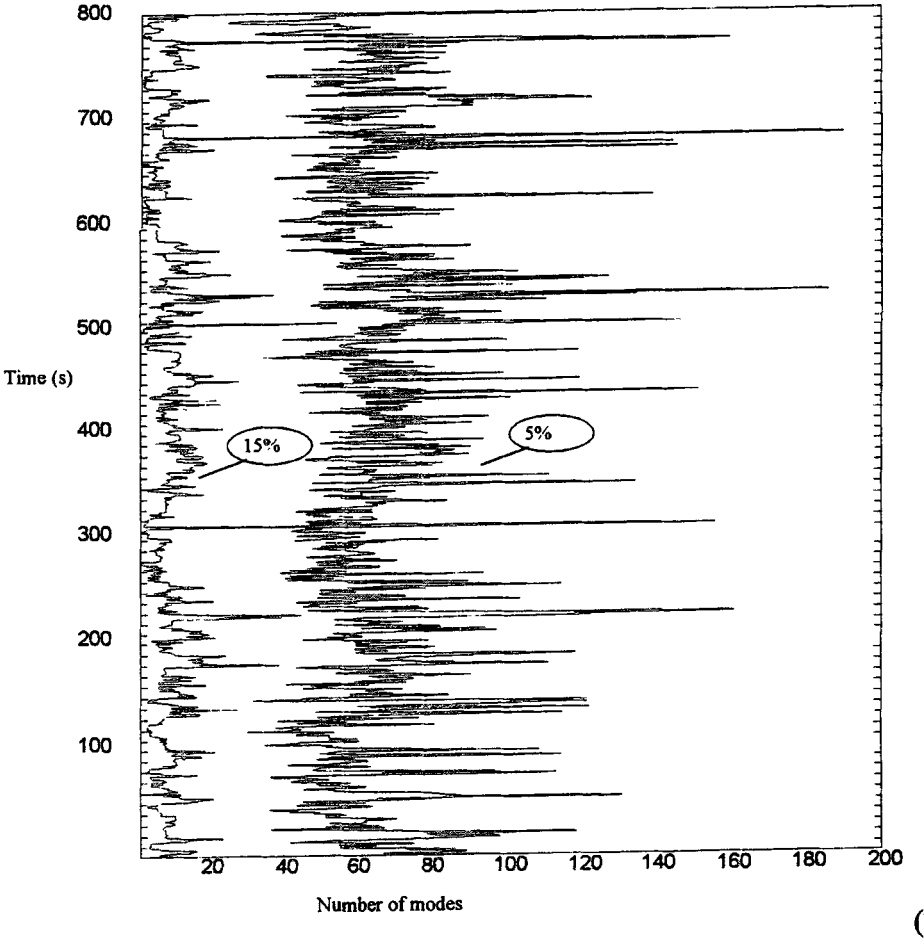

(B)

Figure 9. Percentage errors as a function of the number of modes used to rebuild the field. (A) Time averaged percentage errors, and (B) instantaneous percentage error: isolevels at 15% (left) and 5% (right).

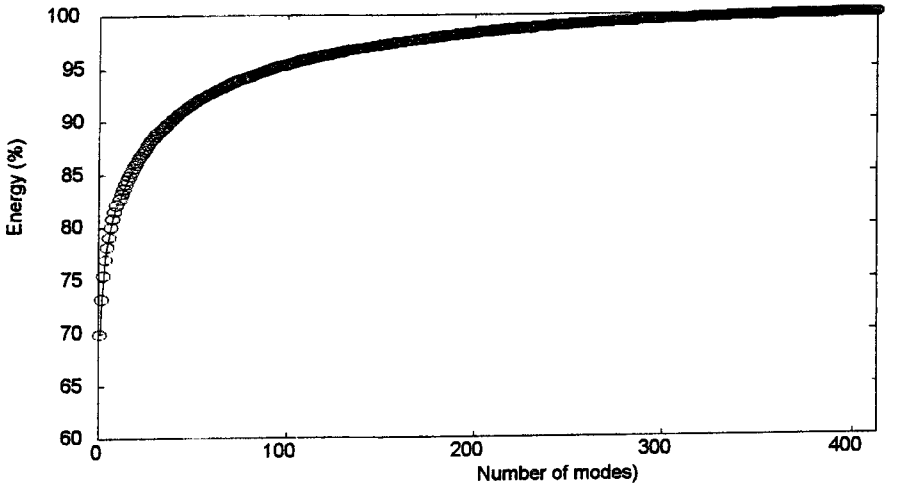

Figure 10. Cumulative energy. The greater amount of energy is retained in the first few modes.

In Figure 10 the cumulative kinetic energy is shown: the first eight modes (1.94% of total number of modes) retain more than 80% of the total energy, while the first 38 modes (9.22%) retain about 90% of the energy.

Modal amplitudes of POD can be regarded as the time evolution of the degree of correlation between velocity field and POD modes. In Figure 11 the time series of the first four amplitudes are plotted: first one is always greater than zero. It does not exhibit any regular behaviour. All the others have mean value close to zero, with periodic oscillations. This is confirmed by the Fourier analysis of the series: power spectra of the first modal amplitude does not show any sharp peak. All the others present two sharp peaks, at two characteristic frequencies: 0.0172 and 0.0577 Hz (Figure 12), corresponding to fluid particle revolution and plume oscillation, respectively.

5. Conclusions and Further Developments

The PTV analysis of convective flow permits very large structures that fill the whole vessel to be shown. Instabilities are driven by velocity perturbations, related to thermal anomalies. These regions of relatively high velocity are detected using a portrait of the vertical component: they are observed travelling alternatively to the left and right side of the tank, following the mean flow. Natural swaying motion of the plume can be related to the transfer of momentum from those regions (hot and cold blobs) to the rolls.

Results of POD analysis give information about structures that are "the best correlated" with velocity fields. Characteristics of these modes were given for a unique case. Our aim is to investigate the behaviour of modes both in space and time domain when control parameters are changed.

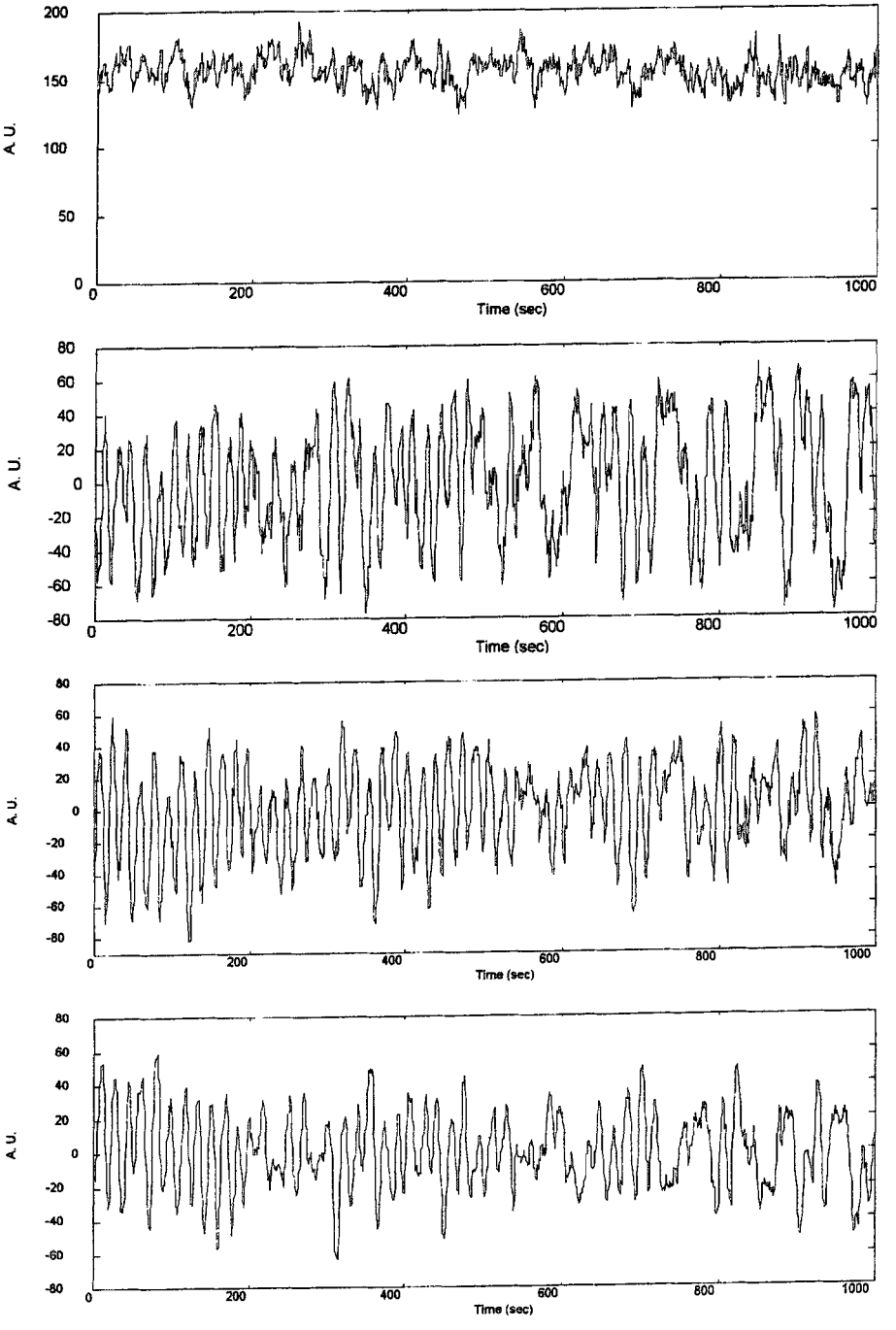

Figure 11. Time series of modal amplitude of the first four modes.

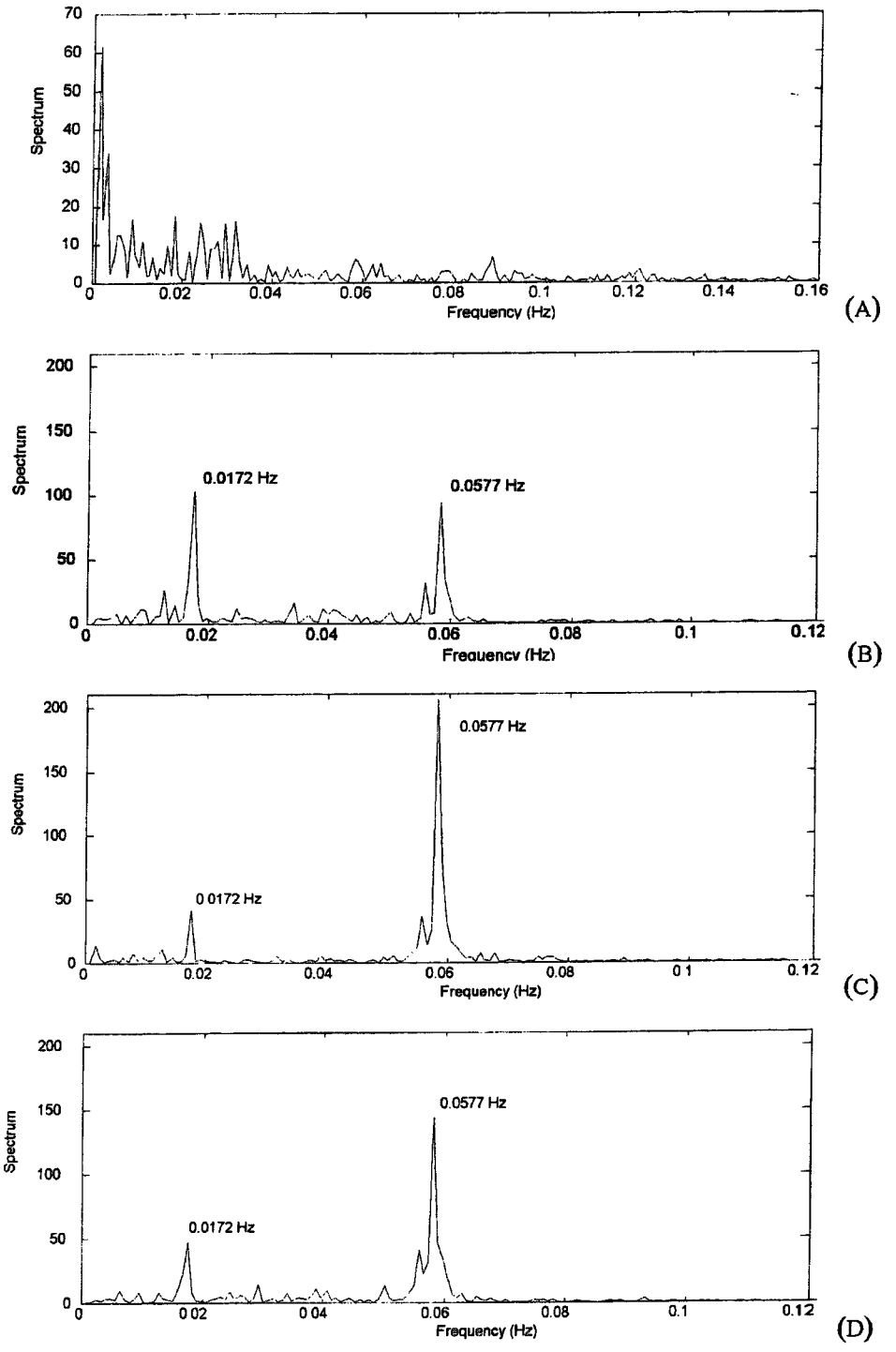

Figure 12. Power spectrum of the first four modes.

Power spectra are localised on characteristic frequencies depending on the grid position. The non-stationary nature of the flow suggests the application of wavelet decomposition to investigate temporal evolution of energy distribution on each point of the grid. Wavelet decomposition gives information both in time and frequency domains simultaneously.

Particle trajectories are given only in the section lighted by the laser sheet: no measurement was performed on the direction of the heating element. Nevertheless, three useful considerations can be made about bi- and tri-dimensionality of the flow fields.

- The experimental set-up breaks the symmetry of the system, resolving indeterminations of the flow in the direction of rolls' axis (like in Rayleigh–Bénard convection, if preferential directions are not imposed by aspect ratios) and about their rotation.
- There are few doubts about the existence of a transversal component of velocity, along the heating element (meandering motion) [21, 22]. But the observation of trajectories of seeding particles, performed on more than 200 consecutive images ($\sim$ three minutes) and the visual observation of the same particle in the light sheet for some time, suggests that flow nature in this experience is at least planar. Transversal component characters are the low values of intensity and the long period of oscillation. Stereoscopic investigations are planned for the future to detect meandering motions together with two-dimensional analysis in sections located near the front and rear walls.
- Despite the planar nature of the flow, observation of velocity anomalies suggests these regions are limited along z-axis: their influence on the flow can be thought of as a function of their position over the heating element. Consequently, the flow can exhibit planar motions that are functions of z-position of the section. This behaviour is planned to be investigated with two colour laser sheets that illuminate two different parallel planes: different colour particles are recorded on different buffers, giving information on different sections at the same time.

References

1. Koschmieder, E.L., *Bénard Cells and Taylor Vortices*. Cambridge: Cambridge University Press (1993).
2. Desrayaud, G. and Lauriat, G., Unsteady confined buoyant plumes. *Journal of Fluid Mechanics* 252 (1993) 617–646.
3. Krishnamurti, R., On the transition to turbulent convection. Part 1. The transition from two- to three-dimensional flow. *Journal of Fluid Mèchanics* 42 (1970) 295–307.
4. Krishnamurti, R., On the transition to turbulent convection. Part 2. The transition to time dependent flow. *Journal of Fluid Mechanics* 42 (1970) 309–320.
5. Moses, E., Zocchi, G. and Libchaber, A., An experimental study of laminar plumes. *Journal of Fluid Mechanics* 251 (1993) 581–601.
6. Lesieur, M., *Turbulence in Fluids*. Dordrecht: Kluwer Academic Publisher (1990).
7. Newell, A.C. and Whitehead, J.A., Finite bandwidth, finite amplitude convection. *Journal of Fluid Mechanics* 38 (1969) 279–303.

8. Berkooz, G., Holmes P. and Lumley J., The proper orthogonal decomposition in the analysis of turbulent flows. *Annual Reviews in Fluid Mechanics* 25 (1993) 539–575.
9. Sirovich, L., Turbulence and the dynamics of coherent structures. Part I: Coherent structures. *Quarterly of Applied Mathematics* XLV(3) (1987) 561–571.
10. Sirovich, L., Turbulence and the dynamics of coherent structures. Part II: Symmetries and transformations. *Quarterly of Applied Mathematics* XLV(3) (1987) 573–582.
11. Sirovich, L., Turbulence and the dynamics of coherent structures. Part III: Dynamics and scaling. *Quarterly of Applied Mathematics* XLV(3) (1987) 583–590.
12. Sirovich, L., Maxey, M. and Tarman, H., An eigenfunction analysis of turbulent thermal convection. In: *Turbulent Shear Flow 6*. Berlin–Heidelberg: Springer-Verlag (1989) pp. 68–77.
13. Deane, A.E. and Sirovich, L., A computational study of Rayleigh Bénard convection. Part 1. Rayleigh number scaling. *Journal of Fluid Mechanics* 222 (1991) 231–250.
14. Lumley, J.L., The structure in inhomogeous turbulence. In: A.M. Yaglom and V.I. Tatarski (eds), *Atmospheric Turbulence and Wave Propagation.* Moscow: Nauka (1967) pp. 166–178.
15. Lumley, J.L., Coherent structures in turbulence. In: R.E. Mayer (ed.), *Transition and Turbulence.* New York: Academic (1981) pp. 215–242.
16. Sirovich, L. and Deane, A.E., A computational study of Rayleigh Bénard convection. Part 2. Dimension consideration. *Journal of Fluid Mechanics* 222 (1991) 251–265.
17. Rajee, M. and Karlsson, S.K.F., Shear flow coherent structures via Karhunen–Loève expansion. *The Physics of Fluids A* 2(12) (1990) 2249–2251.
18. Rajee, M., Karlsson, S.K.F. and Sirovich, L., Free-shear flow coherent structures. *Journal of Fluid Mechanics* 258 (1994) 1–29.
19. Fisher, M. and Wiegel, M., The determination of coherent structures out of PIV data obtained for a transitional boundary layer. Presented at Rome-EUROMECH (1995).
20. Welander, P., On the oscillatory instability of a differentially heated fluid loop. *Journal of Fluid Mechanics* 29 (1967) 17–30.
21. Eichhorn, R. and Vedhanayagam, M., The swaying frequency of line source plumes. In: U. Grigull, E. Hahne, K. Stephan and J. Straub (eds), *Proc. 7th Intl. Heat Transfer Conf.*, Munich. Hemisphere (1982) pp. 407–412.
22. Urakawa, K., Morioka, I. and Kiyota, M., Swaying motion of buoyant plume above a horizontal line heat source. In: *Proc. 1st ASME–JSME Thermal Engineering Conference*, Honolulu HI, Vol. 3 (1983), pp. 215–220.